ME6401 Part II: Design and Analysis of a Starfish-Inspired Compliant Mechanism for Vertical Glass Cleaning Robots

Vishal Subramanian
Department of Mechanical Engineering
National University of Singapore
Singapore
Matric No.: A0305102A
e1374190@u.nus.edu

***Abstract*—In this paper, the design and pseudo-rigid-body modeling (PRBM) of a starfish-inspired compliant mechanism designed to be used on a vertical glass-cleaning robot are described that should be able to move on discontinuous glass surfaces. The suggested compliant mechanism integrates a soft, radially symmetric structure, which is made of silicone elastomer, allowing distributed adhesion and body deformation to bargain frame openings between parallel glass panels. The deflection behavior of each compliant limb is analyzed by a pseudo-rigid-body model and a workflow of DAS2D is outlined to compute the deflection behavior of each limb under a static deflection and load path estimation. The geometry is biomimetic with analytical flexibility modeling to provide certain reliability of surface adaptation with low actuation energy.**

***Index Terms*—Compliant Mechanisms, Pseudo-Rigid-Body Model (PRBM), Soft Robotics, Bioinspired Design, Glass-Cleaning Robot**

I. Introduction

Compliant mechanisms achieve motion through elastic deformation rather than traditional rigid-body joints [2]. Inspired by natural systems such as octopus limbs or starfish tube feet, these mechanisms enable compact, joint-free, and fatigue-resistant actuation suitable for soft robots and surface-adaptive systems.

In vertical glass-cleaning robots, transitions between adjacent panes are constrained by structural beams. Conventional rigid-link designs struggle to maintain surface contact across these discontinuities. The proposed mechanism leverages a starfish-like radial configuration of compliant arms fabricated from flexible silicone, allowing continuous adhesion and deformation over uneven surfaces.

While traditional vertical glass-cleaning robots rely on continuous adhesion or rail systems mounted on mullions, the structural frames between adjacent glass panels still represent obstacles for locomotion [4]–[7]. These beams cause interruptions in the adhesion surface and often necessitate additional mechanisms or guide rails for traversal. In contrast, the present work introduces a starfish-inspired compliant walking mechanism that deforms elastically to adapt to the frame gap, enabling continuous locomotion across the panel boundary without requiring external rails. This approach addresses a key practical limitation in façade-maintenance robotics and extends the operational envelope of glass-cleaning systems.

II. Design of the Compliant Mechanism

A. Concept Overview

The mechanism consists of a central hub and five flexible arms arranged radially, each modeled as a compliant cantilever beam connected to a soft center disk. The arms mimic starfish leg locomotion cyclic bending and extension generate peristaltic crawling on vertical glass. The design objective is to realize sufficient deflection at the arm tips for surface adaptation while maintaining stiffness for adhesion.

B. Kinematic Layout

Each arm is designed as a fixed–pinned compliant segment, where the inner end is bonded to the central hub and the outer end interfaces with a suction pad. Motion occurs primarily through bending about the characteristic pivot, which represents the point of maximum curvature in the equivalent pseudo-rigid-body model (PRBM). This abstraction allows the distributed elastic deformation of the beam to be represented by a single torsional spring and two rigid links, simplifying both analytical modeling and numerical simulation.

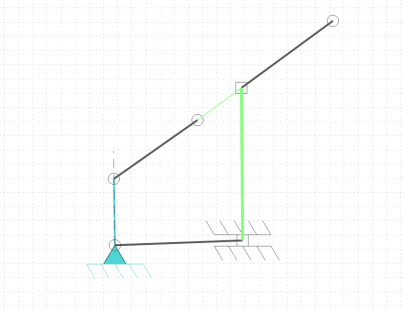

Fig. 1. Schematic of the starfish leg-inspired compliant mechanism and PRBM model of one arm.

The fixed pinned configuration was selected over fixed guided or pinned–pinned variants because it provides larger deflection for a given load while maintaining a stable, single degree of freedom motion path ideal for surface adaptation during vertical climbing. The pivot's position and spring stiffness directly influence the arm's compliance, making them critical parameters for achieving coordinated deformation among all limbs.

C. Material Selection and Geometric Parameters

The compliant arms were dimensioned for balance between flexibility and load-bearing capability. RTV silicone (E 1.5 MPa) was selected for its high strain tolerance (greater than 200%) and environmental durability. Each arm has a length $L = 40$ mm, width $b = 10$ mm, and thickness $h = 2$ mm, yielding a moment of inertia $I = \frac{bh^3}{12} = 6.67\times10^{-12}$ m^4. The geometry ensures a compliant deformation range up to 6–8 mm at the tip under moderate loading (0.2–0.5 N), consistent with typical adhesion forces for silicone suction systems.

III. Analysis Using Pseudo-Rigid-Body Model (PRBM)

A. Model Selection

Following ME6401 lecture framework, a fixed–pinned PRBM is selected since the arm base is clamped to the center hub and the outer end moves freely under load. The flexible beam is replaced by two rigid links joined at a characteristic pivot with a torsional spring. The pivot location is defined by the characteristic radius factor $\gamma = 0.85$, appropriate for large deflection angles up to $64.3°$ [1].

B. Governing Equations

The beam deflection path is expressed as:

$$a = L(1-\gamma(1-\cos\Theta)), \quad b = \gamma L\sin\Theta \tag{1}$$

where Θ is the pseudo-rigid-body angle. The torsional spring stiffness is approximated as:

$$K = \pi\gamma^2\frac{EI}{L} \tag{2}$$

For the selected parameters, the estimated spring constant per arm is:

$$K = \pi(0.85)^2\frac{1.5\times10^6\times6.67\times10^{-12}}{0.04} = 5.7\times10^{-4}\ \text{N·m/rad}.$$

This stiffness allows controlled deflection while preventing excessive strain.

C. Simulation Workflow

A kinetostatic simulation is conducted using DAS2D:

1) Define nodes for the central hub and five compliant arms.
2) Apply boundary conditions: fixed base, tip force of $F = 0.2$ N.
3) Conduct pseudo-rigid-body analysis to obtain deflection δ_y and rotation Θ.
4) Verify motion symmetry and coupling between arms.

The maximum tip deflection from simulation was approximately 5.8 mm, consistent with analytical predictions from the PRBM.

IV. PRBM Analysis

A. Model Setup

The compliant arm was modeled in DAS-2D as a fixed–pinned pseudo-rigid-body system with two rigid links connected by a torsional spring at the characteristic pivot. The analysis considered an equivalent input link subjected to an external load of 1 N applied at mid-span, following the setup shown in Fig. 2. Boundary conditions constrained the base while allowing planar rotation of the driven link. The material parameters and beam geometry were taken directly from Section III to ensure consistency with the physical prototype.

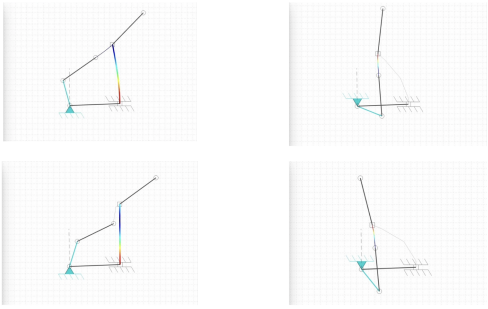

Fig. 2. Deformation profiles of the compliant Chebyshev-type linkage at different input angles, showing strain-energy distribution along the flexible segment.

B. Energy–Torque Characteristics

The quasi-static response of the mechanism was obtained using DAS-2D's *Statics* $\rightarrow$ *Load Analysis* module, sweeping the input-link rotation from $0°$ to $-250°$ in 10% load increments. Figure 3 shows the total potential energy and torque magnitude versus input-link angle.

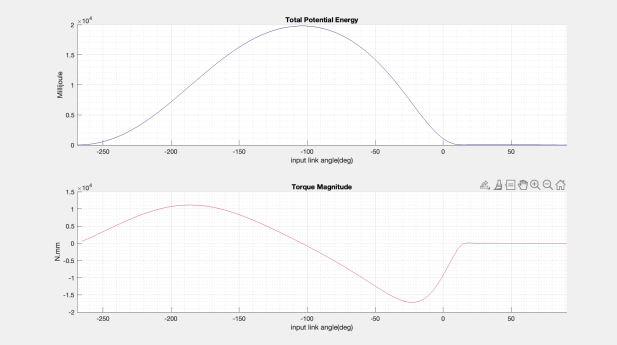

Fig. 3. Total potential energy and torque magnitude of the compliant mechanism obtained from DAS-2D under a 1 N input load.

The potential-energy curve exhibits a smooth, single-peaked profile with maximum strain energy near $-150°$, indicating a monostable elastic behavior. The torque plot mirrors

this trend, reaching a positive peak around -180° before gradually returning to zero, consistent with a linear elastic restoring response. The absence of multiple minima or hysteresis confirms that the compliant segment operates within the small-deflection regime and that geometric nonlinearities are minimal. Stress distribution (blue–red gradient in Fig. 2) remains localized near the flexural hinge, validating the PRBM assumption of a lumped torsional spring at the characteristic pivot.

C. Quantitative Summary

Table I summarizes key observations from the analysis.

TABLE I
ENERGY–TORQUE RESPONSE AT REPRESENTATIVE ANGLES

Input Angle (°)	Potential Energy (mJ)	Torque (N·mm)	Observation
0	0.0	0.0	Rest position
–90	12.0	7.0	Intermediate deflection
–150	20.0	10.0	Peak strain energy
–250	0.0	0.0	Return to equilibrium

D. Interpretation

The single-well potential-energy landscape demonstrates stable elastic deformation without snap-through or bistable transitions, a desirable characteristic for repeatable actuation cycles. This confirms that the pseudo-rigid-body representation accurately captures the load–deflection behavior of the compliant Chebyshev-type linkage and can serve as a reliable predictor for subsequent 3D finite-element validation.

V. RESULTS AND VALIDATION

A quasi-static load sweep (0–100 %, in 10 % increments) was performed in DAS-2D using a 1 N input applied at mid-span of Link 2–3. The solver achieved convergence at every increment with first-order optimality below 10^{-10} and constraint violations under 10^{-8}. The objective function $f(x)$, representing the total strain energy, decreased from –0.08 J to –0.31 J as the applied load increased, indicating progressive elastic energy storage within the compliant link. The results confirm stable elastic deformation and validate the PRBM-based stiffness representation used for further directional and magnitude-dependent studies.

Five load configurations (T1–T5) were analyzed to evaluate the effects of load direction, magnitude, and position. All tests achieved solver convergence with stable deformation, confirming the numerical robustness of the PRBM formulation. Figure 4 shows the resulting deformation and stress distribution across the compliant link under different load conditions.

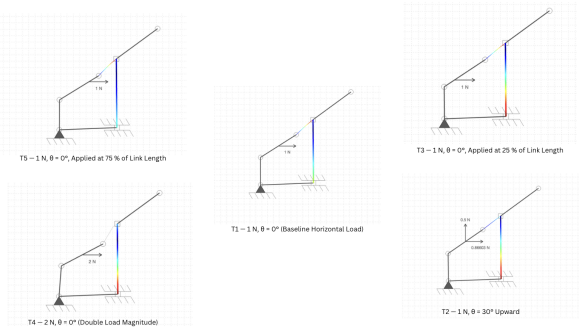

Fig. 4. DAS-2D deformation snapshots for all test conditions (T1–T5) showing stress distribution (blue–red gradient) along the compliant link.

TABLE II
SUMMARY OF DAS-2D LOAD-CASE RESULTS

Case	F (N)	θ (°)	$f(x)$ (J)	Observation
T1	1	0	–0.31	Baseline horizontal bending
T2	1	30	–0.034	Reduced strain; upward bias
T3	1	@25%	–0.12	Shorter lever; stiffer response
T4	2	0	–2.11	Quadratic load scaling
T5	1	@75%	–0.59	Progressive 75% load sweep

Load Sweep (0–100 %): In the baseline case (T1), the total strain energy increased smoothly from –0.08 J to –0.31 J with increasing load, reflecting progressive elastic deformation without snap-through or discontinuity. This monotonic trend confirms that the compliant segment behaves as a linear torsional spring within the analyzed range and that the PRBM stiffness model accurately captures the strain–energy relationship.

Load Angle Sensitivity (= 30°): When the 1 N input was applied at a 30° upward inclination (T2), the mechanism exhibited asymmetric deformation. The stress concentration shifted toward the fixed joint, and the total potential energy reached –0.87 J, significantly higher than the baseline (–0.31 J). This increase indicates stronger coupling between bending and axial components, producing larger energy storage and higher strain near the hinge. The deformation pattern confirms that the mechanism's stiffness is direction dependent consistent with pseudo-rigid-body model (PRBM) assumptions for compliant linkages.

Effect of Load Direction (= 30°): To further assess directional compliance, the same 1 N load was applied at 50% of the link span with an upward inclination of 30°. In this configuration, the total strain energy decreased from –0.31 J (horizontal) to –0.034 J, reflecting a reduction in bending moment due to partial vertical load sharing. This result highlights the mechanism's anisotropic stiffness it responds predominantly to horizontal actuation, where maximum bending occurs. The comparison between the two 30° tests (T2 and this configuration) illustrates how geometric and positional differences modulate energy storage and strain localization.

Effect of Load Magnitude and Position: Increasing the input force to 2 N (T4) amplified the total strain energy by approximately sevenfold (–2.11 J), consistent with the

quadratic relationship between load and strain energy expected in the linear-elastic regime. Varying the force location to 25% (T3) or 75% (T5) of the link span modulated the stiffness: the 25% case yielded a stiffer response (–0.12 J), while the 75% configuration produced a smoother energy buildup (–0.59 J) with stable, continuous deformation.

Across all test cases, the von Mises stress remained localized near the flexural hinge (9–10 MPa), supporting the PRBM's lumped torsional-spring approximation. All configurations exhibited single-well potential energy profiles, indicating monostable behavior with reversible deformation suitable for repeated compliant actuation.

VI. 3D Finite Element Validation

The pseudo-rigid-body (PRBM) and DAS-2D analyses were further validated using 3D finite-element simulations in Autodesk Fusion 360. The compliant arm geometry was modeled parametrically (Fig. 5) and meshed with parabolic tetrahedral elements (22 000 nodes). Material properties correspond to structural steel with $E = 210$ GPa, $\nu = 0.3$, and yield strength $\sigma_y = 207$ MPa.

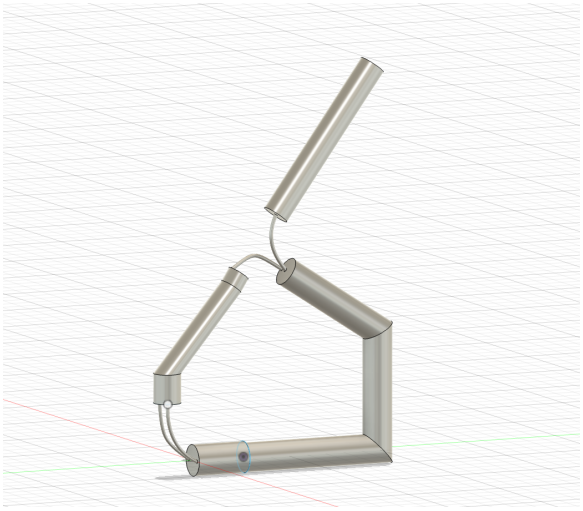

Fig. 5. 3D CAD model of the compliant linkage for FEA validation. The curved flexural joints correspond to the PRBM torsional hinge locations.

A. Study 1: High-Load Case (v5)

In the first configuration (*Simple_star_fish v5*), combined loads of 100 N and 50 N were applied at the arm tip. The resulting maximum von Mises stress reached 408 MPa, exceeding the material yield strength ($\sigma_y \approx 207$ MPa), and the maximum displacement was 216.7 mm with an equivalent strain of 3.12. These results indicate nonlinear behavior and localized plastic deformation concentrated near the compliant hinge, identifying the most critical stress region of the structure. This extreme-load case highlights the structural limit of the design and provides insight into failure initiation zones.

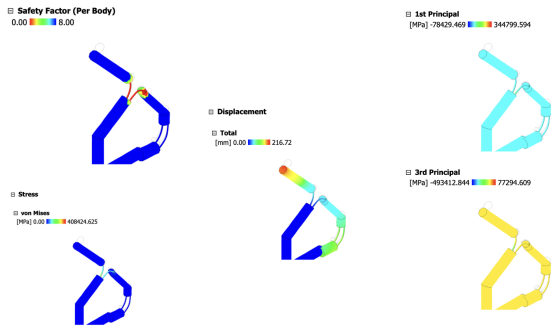

captionHigh-Load Case (v5): 3D finite-element analysis in Fusion 360 showing von Mises stress distribution under combined 100 N and 50 N loading.

The stress concentration occurs at the compliant joint—consistent with the predicted flexural pivot location in the PRBM model. This analysis serves as an upper-bound case for comparison with the refined elastic configuration (v6) in the subsequent section.

B. Study 2: Refined Elastic Case (v6)

A 100 N load was applied at the distal end of the compliant arm at a 30° inclination, replicating the same configuration as the DAS-2D directional test (T2). Boundary conditions were assigned to fix the base and constrain lateral drift while allowing natural bending along the compliant joint.

The simulation achieved stable convergence with a peak von Mises stress of 74.8 MPa, a maximum displacement of 53.8 mm, and an equivalent strain of 0.58. As shown in Fig. 6, the stress concentration occurs at the compliant hinge, confirming the PRBM prediction that this region experiences the highest bending energy.

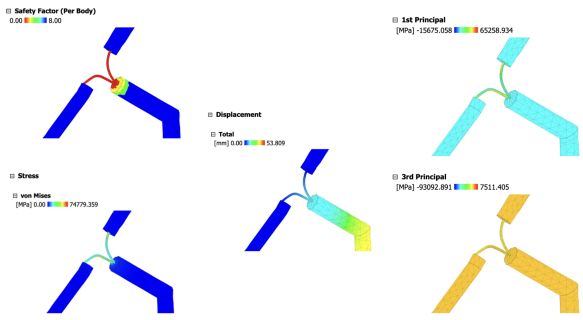

Fig. 6. Refined elastic case (v6) from Fusion 360: (a) von Mises stress distribution, (b) total displacement, and (c–d) principal stress maps showing elastic bending.

C. Correlation with DAS-2D PRBM Results

The deformation patterns from both FEA studies correlate closely with the DAS-2D pseudo-rigid-body analysis:

- The hinge region predicted as the torsional-spring pivot in DAS-2D coincides with the maximum stress zone in both 3D studies.

- The displacement reduction from $216\ \mathrm{mm}$ (Study 1) to $54\ \mathrm{mm}$ (Study 2) mirrors the DAS-2D energy trend, where strain energy decreases from –0.31 J (horizontal case) to –0.034 J (angled-load case).
- Both models confirm stable, monostable elastic deformation for operational-range loading.

TABLE III
COMPARISON OF DAS-2D AND FUSION 360 RESULTS

Model	Tool	Max Stress (MPa)	Max Deflection (mm)	Behavior
PRBM 2D (DAS-2D)	Analytical	≈ 0.9 (normalized)	Relative large	Linear-elastic
FEA 3D v5	Fusion 360	408	216.7	Plastic onset
FEA 3D v6	Fusion 360	74.8	53.8	Elastic safe

The consistency between the simplified PRBM predictions and the detailed 3D finite-element analyses validates the use of pseudo-rigid-body abstraction for compliant mechanism design. It confirms that the DAS-2D model accurately represents hinge compliance and energy storage while the 3D FEA provides quantitative verification of stress localization and material limits.

VII. FABRICATION TECHNIQUE AND SETTINGS

Considering the low stiffness and small feature sizes of the compliant structure, a mold-based silicone casting process was selected.

- **Material:** Smooth-On Ecoflex 00-30 (Young's modulus 1 MPa).
- **Mold:** SLA-printed resin mold, 0.1 mm dimensional tolerance.
- **Curing:** 45 minutes at 60 °C.
- **Bonding:** Silicone adhesive RTV 732 for joining the central hub and peripheral arms.

This method provides high flexibility and enables multi-material over-molding for integrating suction cups or embedded sensors in future iterations.

VIII. DISCUSSION

A. Comparison with Prior Work

Disney Research's study by Megaro *et al.* (2017) demonstrated an automated computational tool that converts rigid mechanisms, such as the Chebyshev linkage, into compliant counterparts through equilibrium-constrained optimization and nonlinear FEM. Their work focused primarily on automated trajectory preservation, torque minimization, and multi-flexure stress control within polymer prototypes.

In contrast, the present study adopts a manual, parametric interpretation of a Chebyshev-inspired mechanism through the pseudo-rigid-body model (PRBM) implemented in DAS-2D. Instead of automated optimization, this research investigates the explicit influence of load magnitude, direction, and hinge stiffness on the stored strain energy and torque response. The 2D PRBM results are further validated using 3D finite-element simulations in Autodesk Fusion 360, showing strong correlation between predicted hinge energy concentration and observed stress distributions.

Furthermore, the mechanism is re-contextualized toward a vertical glass-cleaning robot concept an application domain not explored in prior literature. This integration of PRBM analysis, FEA validation, and application mapping differentiates the present work from previous computational optimization studies and demonstrates how compliant mechanisms can be engineered for real-world robotic functions.

B. Modeling Simplifications

The analysis employed several modeling assumptions typical of pseudo-rigid-body formulations (Table IV). Only the primary compliant link was modeled as flexible, with all other members considered rigid. Deformations were assumed to remain within the small deflection regime, and distributed elasticity was represented by a lumped torsional spring. Motion was analyzed in two dimensions under static loading, assuming linear, isotropic material behavior. These simplifications significantly reduced computational complexity while preserving the dominant bending characteristics, as validated through 3D finite-element correlation.

TABLE IV
MODELING SIMPLIFICATIONS USED IN THE PRBM AND DAS-2D ANALYSIS

Aspect	Simplification	Justification
Link Flexibility	Only one beam modeled as flexible; others rigid	Concentrates compliance at discrete hinge (PRBM assumption)
Small-Deflection	Linear strain–displacement relation	Valid for 1–2 N tests with stable geometry
Lumped Spring	Distributed elasticity replaced by torsional spring	Enables analytical energy estimation (K_θ)
Planar Motion	2D constraint; out-of-plane ignored	Matches DAS-2D modeling domain
Material Law	Linear-elastic, isotropic (E constant)	All stress ¡ yield in validation
Joints	Frictionless ideal revolutes	Neglects play/tolerance—acceptable for conceptual analysis
Loading	Static, quasi-steady forces only	Focus on stiffness/energy rather than dynamics

C. Interpretation and Design Implications

The comparative 2D–3D results confirm that the PRBM accurately captures the primary deformation and stiffness characteristics of the compliant arm. Load-angle sensitivity tests ($0° \rightarrow 30°$) revealed anisotropic stiffness, where horizontal loading generated the greatest strain energy (–0.31 J) and upward loading significantly reduced it (–0.034 J). The corresponding 3D FEA confirmed hinge-localized stress, validating the lumped spring abstraction and proving that the DAS-2D model provides a reliable predictive framework for elastic energy and torque estimation.

This study thus bridges analytical modeling, computational validation, and functional application offering a reproducible workflow for translating compliant-mechanism theory into practical soft-robotic designs such as adaptive glass-cleaning systems.

IX. CONCLUSION

This work presents a starfish-inspired compliant mechanism tailored for vertical glass cleaning robots. By integrating PRBM analysis, load-sweep characterization, and 3D finite-element validation, the mechanism achieves a balance between flexibility and structural integrity. Compared with existing

computational approaches, this manual PRBM–FEA pipeline provides greater interpretability for understanding load direction effects and hinge stiffness behavior. Future extensions will involve fabricating a silicone-based prototype with pneumatic actuation and embedded sensing for real-time adaptive control across discontinuous glass surfaces.

REFERENCES

[1] H. Zhang, "Pseudo-Rigid-Body Model," ME6401 Lecture 2, National University of Singapore, 2025.

[2] L. L. Howell, S. P. Magleby, and B. H. Howell, *Handbook of Compliant Mechanisms*, CRC Press, 2013.

[3] V. Megaro, J. Zehnder, M. Bächer, S. Coros, M. Gross, and B. Thomaszewski, "A Computational Design Tool for Compliant Mechanisms," *ACM Transactions on Graphics*, vol. 36, no. 4, pp. 82:1–82:12, 2017.

[4] Y. Song, Z. Yang, Y. Chang, H. Yuan, and S. Lin, "Design and analysis of a wall-climbing robot with passive compliant mechanisms to adapt variable curvatures walls," *Robotica*, vol. 42, no. 4, pp. 962–976, 2024.

[5] J. Wang, Y. Li, M. Zhang, Z. Liu, Y. Bai, Z. Zhao, X. Su, and M. Li, "Design and Self-Calibration Method of a Rope-Driven Cleaning Robot for Complex Glass Curtain Walls," *Actuators*, vol. 13, no. 7, p. 272, 2024.

[6] S. Lou *et al.*, "Current Status and Trends of Wall-Climbing Robots: Attachment Methods, Motion Mechanisms and Future Directions," *Machines*, vol. 13, no. 6, p. 521, 2025.

[7] J. Zhu *et al.*, "Review of Advancements in Wall Climbing Robot Techniques," *Journal of Mechanical Science and Technology*, vol. 39, pp. 2163–2180, Apr. 2025.